RSC Advances

PAPER

View Article Online
View Journal | View Issue

Cite this: *RSC Adv.*, 2025, **15**, 36969

Effective electrochemical synthesis of ferrate(VI) utilizing a porous iron foam anode and its application in the removal of azo dye reactive red 24

Thi Van Anh Nguyen,[a] Thi Xuan Mai,[a] The Duyen Nguyen,[c] Minh Quy Bui,[d] Hoang Yen Phan[e] and Thi Thanh Thuy Mai*[ab]

Received 22nd July 2025
Accepted 22nd September 2025

DOI: 10.1039/d5ra05299h

rsc.li/rsc-advances

Anode passivation is a significant challenge in the electrochemical synthesis of ferrate(VI), resulting in diminished Fe(VI) production efficiency. In this study, cyclic voltammetry (CV), electrochemical impedance spectroscopy (EIS), scanning electronic microscopy (SEM), X-ray diffraction (XRD), energy-dispersive X-ray spectroscopy (EDS), and *E*–*t* polarization curves were used to evaluate the electrochemical properties and the formation of passivation layers on two anode materials, namely, pure iron (PI) and porous iron foam (PIF). Results revealed that PIF had favorable characteristics for ferrate(VI) generation, such as improved electron transfer capability and mitigated anode passivation compared with PI. Experiments also confirmed that PIF significantly outperformed PI in ferrate(VI) synthesis, achieving a synthesis efficiency of up to 63% in 14 M NaOH solution. The synthesized ferrate(VI) was subsequently applied to the treatment of the dye reactive red 24 (RR24), yielding a high removal efficiency of up to 98% at a ferrate/RR24 mass ratio of 2 g g^{-1}.

1. Introduction

The direct discharge of untreated domestic wastewater and industrial wastewater, particularly from textile dyeing and pharmaceutical processes, into the environment is considered one of the major causes of global surface water pollution. These types of wastewaters typically contain a complex mixture of organic dyes, toxic chemicals, heavy metals, and reactive nitrogen, which severely degrades the water quality and disrupts the aquatic ecosystems.[1–5] The presence of these contaminants also poses significant health risks.[6,7]

Among various organic dyes, azo dyes, such as reactive red 24 (RR24), are highly toxic and resistant to biodegradation, making their removal from wastewater particularly challenging. Traditional methods like coagulation–flocculation, adsorption, and biological treatment often have limited efficiency for such persistent dyes and may generate secondary pollution or require long processing times. Ferrate(VI) (FeO_4^{2-}), a powerful and environmentally friendly oxidant, has recently gained attention as a promising alternative.[6,8] It can effectively oxidize a wide range of organic pollutants and decompose into Fe(III), which aids in the coagulation and removal of suspended solids, while also facilitating disinfection and heavy metal removal.[9,10] Previous studies have demonstrated ferrate's effectiveness in treating various dyes, with removal efficiencies over 90% depending on the dye type and dosage.[11–13] However, only limited studies have yet evaluated the application of ferrate(VI) for the treatment of the azo dye reactive red 24.

Ferrate can be synthesized by three main methods: dry synthesis, wet chemical synthesis, and electrochemical synthesis.[14,15] Among these, the electrochemical approach offers several advantages due to its simple, environmentally friendly process. Notably, it enables *in situ* ferrate generation for direct application in water and wastewater treatment, addressing ferrate's inherent instability.[16] In electrochemical synthesis, the choice of the anode material and electrolyte composition plays a critical role in determining the efficiency of ferrate production. Commonly used anode materials in the electrochemical synthesis of ferrate are iron and its alloys, such as white cast iron, grey cast iron, and steel. Numerous studies have demonstrated that the chemical composition of the anode material significantly influences the formation of a passive layer—a non-conductive oxide film that is formed on the anode surface. This passive layer prevents the oxidation of Fe(III) to Fe(VI), thereby reducing the overall ferrate yield.[17–19] In particular, the presence of elements such as silicon or carbon in the anode material reduced the stability of the passive layer.[20–22] According to M.

---

[a] *Institute of Chemistry, Vietnam Academy of Science and Technology, 18 Hoang Quoc Viet, Nghia Do, Hanoi, 10072, Vietnam. E-mail: thuyttmai@ich.vast.vn*
[b] *Graduate University of Science and Technology, Vietnam Academy of Science and Technology, 18 Hoang Quoc Viet, Nghia Do, Hanoi, 10072, Vietnam*
[c] *Faculty of Chemistry, Hanoi Pedagogical University 2, Xuan Hoa, Phu Tho, Vietnam*
[d] *Faculty of Chemistry, TNU – University of Sciences, Thai Nguyen, Vietnam*
[e] *Faculty of Natural Sciences, Electric Power University, Hanoi, Vietnam*

Čekerevac *et al.*,[22] silicon reacted with oxidation products to form soluble silicate compounds in alkaline media, limiting the accumulation of the passive layer on the electrode surface. In addition to chemical composition, the porosity of the anode material is a key factor affecting the efficiency of electrochemical ferrate synthesis. Previous research demonstrated that increasing the porosity of the electrode reduces iron passivation and increases iron dissolution. Xuhui Sun *et al.*[17] utilized sponge iron and grey cast iron as anodes for ferrate electrochemical synthesis. The results indicated that the ferrate yield using sponge iron anodes was higher than that using grey cast iron anodes due to a larger surface area and porosity, resulting in less passive layer formation. In ref. 23, the authors used a porous magnetite electrode to electrogenerate ferrate. The ferrate yield achieved a relatively high 52.3% at 30 °C after 5 hours of electrolysis; however, the passive layer formation was not completely prevented. Similarly, our previous research demonstrated that the porous graphite structure in ductile cast iron anodes contributed to increased ferrate formation by enabling deeper penetration of the electrolyte into the anode structure.[18] These findings indicate that material porosity is an important criterion for selecting anode materials in electrochemical ferrate synthesis. When comparing the porosity of materials such as PIF, sponge iron, and gray cast iron with different microstructures, sponge iron exhibits non-uniform porosity, which is attributed to its low-temperature, solid-state reduction process.[24] Porosity is considered a detrimental defect in gray cast iron. Meanwhile, the porosity value of PIF is dramatically higher than those of sponge iron, typically ranging from 95% to 98%. Besides its excellent porosity, as a metal foam, PIF possesses high electrical conductivity, mass transfer efficiency, and permeability, making it suitable for use as an electrode material.[25] Furthermore, due to its large surface area, PIF is highly predisposed to corrosion; this disadvantage is offset by its susceptibility to oxidation to create ferrate. Thus, among the potential anode materials, porous iron foam-a material that has not yet been used in ferrate synthesis—possesses a high specific surface area, which is favorable for enhancing ferrate generation *via* electrochemical processes.

In addition, the type of electrolyte is a critical factor influencing the efficiency of ferrate synthesis. Sodium hydroxide (NaOH), potassium hydroxide (KOH), or a mixture of NaOH and KOH solutions have been employed in previous studies, depending on the type of anode material used. Several studies have shown that white cast iron performs better in KOH media, whereas gray cast iron, steel, and pure iron tend to yield higher efficiency in NaOH solutions.[21,26] Other researchers have chosen to use a mixture of these two strong bases to optimize the ferrate synthesis efficiency.[27,28]

This study focuses on the electrochemical synthesis of ferrate using porous iron foam (PIF) as the anode material and comparing it to pure iron (PI). The primary objectives are (i) to evaluate whether using PIF anodes can enhance ferrate(VI) yield by mitigating passive layer formation and (ii) to evaluate the effectiveness of the synthesized ferrate for degrading the azo dye RR24. To achieve these, the anodes were tested in three types of electrolytes: 14 M NaOH, 14 M KOH, and a NaOH/KOH mixture with a total OH^- concentration of 14 M. The analytical methods used include cyclic voltammetry (CV) and electrochemical impedance spectroscopy (EIS) to analyze the electrochemical properties. SEM, EDS, XRD, and potential–time (*E*–*t*) curves were used to examine the formation of the passive layer in detail. UV-vis spectroscopy was used to measure the concentration of the RR24 dye before and after treatment, quantifying the efficiency of the ferrate for dye removal.

2. Experimental

2.1 Chemicals and materials

All chemicals including sodium hydroxide (NaOH), potassium hydroxide (KOH), and reactive red 24 were purchased from Sigma-Aldrich (USA). The porous iron foam-PIF with 99.99% Fe (from Tan Qian Lang, China) and pure iron-PI with 99.7% Fe (from Hanoi Mechanical Limited Company, Vietnam) were used for the fabrication of the working electrodes.

2.2 Research and synthesis methods

All experiments related to ferrate synthesis and electrochemical measurements were carried out on an IM6 electrochemical workstation (Zahner Elektrik, Germany) in a conventional three-electrode setup comprising a titanium counter electrode, an Ag/AgCl reference electrode, and a working electrode (PI or PIF). Ferrate(VI) was synthesized by galvanostatic method in concentrated alkaline media. During the synthesis process, the cathode and anode chambers were separated using an Ultrex CMI-7000 cation exchange membrane (USA). The electrochemical properties of the working electrodes were characterized using electrochemical impedance spectroscopy, with a 5 mV amplitude over a frequency range from 100 kHz to 10 mHz, and cyclic voltammetry at a scan rate of 150 mV s^{-1} in the potential range of −1.6 to +0.6 V *vs.* Ag/AgCl.

The influence of the current density on the ferrate concentration and synthesis efficiency was investigated over a 1 hour electrolysis period at ambient temperature (20 °C) in different electrolytes, including 14 M NaOH, 14 M KOH, and a NaOH/KOH mixture (total $[OH^-] = 14$ M and mole ratio Na/K = 1/1). To examine the effect of temperature, experiments were performed in 14 M NaOH for 1 hour, using optimized current densities for the PI and PIF anodes. The impact of the electrolysis duration on the ferrate concentration and synthesis efficiency was further studied under the conditions of 14 M NaOH, 40 °C, with the optimized current densities for the PI and PIF anodes.

The obtained ferrate concentration was determined by UV-vis method using the DR 6000 spectrophotometer (Hach, USA). The anode surface's morphology, composition, and phase structure before and after ferrate electro-generation were determined by SEM images and EDS on the equipment FE-SEM Hitachi S-4800 (Japan), XRD on a D8-ADVANCE (Germany) system.

2.3 Reactive red 24 treatment

A 50 mg L^{-1} RR24 dye solution was treated with the synthesized ferrate. First, the synthesized ferrate was mixed with the dye solution. After mixing, the solution was stirred at 400 rpm for 5 minutes and then left to settle. To determine the optimal pH for RR24 degradation, the pH of the mixed solution was adjusted to 1, 3, 6, and 9. The dye treatment process was investigated by two dosing methods: a single-dose (SD) and multiple-dose (MD) addition. In the SD addition, the entire amount of ferrate was added at once to the dye solution. In the MD addition, the total added ferrate was divided into smaller portions, with each dose corresponding to a ferrate/RR24 mass ratio of 0.5 g g^{-1}. To determine the required amount of ferrate for treating RR24 dye, the ferrate-to-RR24 mass ratio was investigated from 0.5 to 2.5 g g^{-1} using the MD procedure. The concentration of the produced ferrate and dye before and after treatment was measured by optical absorption on the DR 6000 spectrophotometer (Hach, USA).

2.4 Calculations

Ferrate electro-generation efficiency (η) can be calculated by eqn (1):

$$\eta = \frac{n_{\text{actual}}}{n_{\text{theoretical}}} \times 100\% \tag{1}$$

where n_{actual} is the actual molarity of the produced ferrate and calculated by eqn (2), and $n_{\text{theoretical}}$ is the theoretical molarity of ferrate and calculated by Faraday's laws:

$$n_{\text{actual}} = C_{\text{ferrate}} \times V \tag{2}$$

where C_{ferrate} is the concentration of ferrate (in mol L^{-1}) and V is the electrolyte volume (in L):

$$n_{\text{theoretical}} = \frac{I \cdot t}{n \cdot F} \tag{3}$$

where I is the current (in A), t is the electrolysis time (in s), n is the number of electrons transferred (for ferrate(VI), $n = 6$), and F is Faraday's constant (96 485 C mol^{-1}).

The RR24 removal efficiency (R(%)) was calculated following eqn (4)

$$R = \frac{C_0 - C_t}{C_0} \times 100 \tag{4}$$

where C_0 is the initial RR24 concentration (mg L^{-1}) and C_t is the residual RR24 concentration (mg L^{-1}) after a time (t) of RR24 removal.

3. Results and discussion

3.1 Cyclic voltammetry and electrochemical impedance spectroscopy study

To clarify the electrochemical reactions occurring during the oxidation of Fe(0) to ferrate (Fe(VI)) in highly concentrated alkaline media, CV curves of the PIF and PI anodes were recorded in different electrolytes (KOH, NaOH, and a mixed NaOH/KOH solution with a molar ratio of Na/K = 1) with a OH$^-$ concentration of 14 M and in the potential window of −1.6 to 0.6 V (*vs.* Ag/AgCl). The results given in Fig. 1 and 2 indicate that there are four oxidation peaks and shoulder (O1, O2, O3, and O4) on the anode branch and four reduction peaks (R1, R2, R3, and R4) on the cathode branch. All oxidation peaks and shoulder correspond to successive changes of the oxidation state of iron on the anode surface, as described by the Pourbaix diagram, in a highly alkaline environment. The oxidation sequence occurs with increasing potential as follows: Fe → Fe(II) → Fe(II/III) → Fe(III) → Fe(VI).[18,29] Specifically, the O1 peak is characteristic of the oxidation of Fe to FeO, while the O2 peak indicates the oxidation of FeO to Fe_3O_4. The O3 peak represents the oxidation of Fe_3O_4 to Fe_2O_3, and the O4 peak shoulder corresponds to the oxidation of Fe_2O_3 to FeO_4^{2-}.[20,30] The reduction peaks correspond to the reverse processes: Fe(VI) → Fe(III) (R4), Fe(III) → Fe_3O_4 (R3), Fe_3O_4 → Fe(II) (R2), and Fe(II) → Fe (R1).[20,30] If the intermediate products (FeO, Fe_3O_4, Fe_2O_3) do not fully convert into ferrate, they may form a passivation layer on the anode surface, hindering further electrochemical reactions.[17,19,21] The O4 peak shoulder appears in the potential region where oxygen evolution occurs, indicating a competition between ferrate formation and water electrolysis on the anode surface.

Fig. 1a–c show that the intensities of the redox peak pairs corresponding to intermediate formation, (O1, R1), (O2, R2), and (O3, R3), gradually increase over successive scan cycles in all electrolyte solutions for the PI anode. For example, in the NaOH/KOH electrolyte, the maximum current density at peak O3 is 3.8 mA cm^{-2} in the second cycle. After 50 cycles, the height of this peak is 8.5 mA cm^{-2}, which is more than double that of the second cycle. However, the (O4, R4) peak pair, representing ferrate formation, remains nearly unchanged. This evidence indicates a progressive accumulation of a passivation layer on the surface of the PI anode with increasing scan cycles. In contrast, for the PIF anode (Fig. 2a–c), the intensities of all four redox peak pairs remain relatively stable across multiple cycles, demonstrating its electrochemical stability over time. For instance, in the NaOH solution, the current density of the O_2 and O_3 peaks was about 31.0 and 38.3 mA cm^{-2} at the second cycle, respectively, and remained unchanged after 50 cycles.

Fig. 1d and 2d show the CV spectra of PI and PIF at the 50th cycle in NaOH, KOH, and mixed NaOH/KOH electrolytes. The results consistently demonstrate a higher current density response in the oxygen evolution reaction (OER) region for both KOH and NaOH/KOH solutions compared to NaOH alone. This suggests superior ionic conductivity in the KOH-containing electrolytes. This phenomenon is attributed to the distinct atomic radii and hydration properties of sodium (Na^+) and potassium (K^+) ions.[31,32] The larger ionic radius of the K^+ ion compared to the Na^+ ion results in a lower charge density for the K^+ ion. Consequently, K^+ ions interact less strongly with water molecules and form a less stable hydration shell than Na^+ ions.[33] The weaker hydration of the K^+ ion allows it to be less encumbered by its hydration shell; it can move more freely through the solution. This higher mobility of the K^+ ion leads to a higher overall conductivity for KOH solutions compared to NaOH solutions of the same concentration.[33] Therefore, oxygen release is more pronounced in electrolytes containing KOH than NaOH. This increased oxygen evolution may hinder the generation of ferrate, as this process occurs in the OER

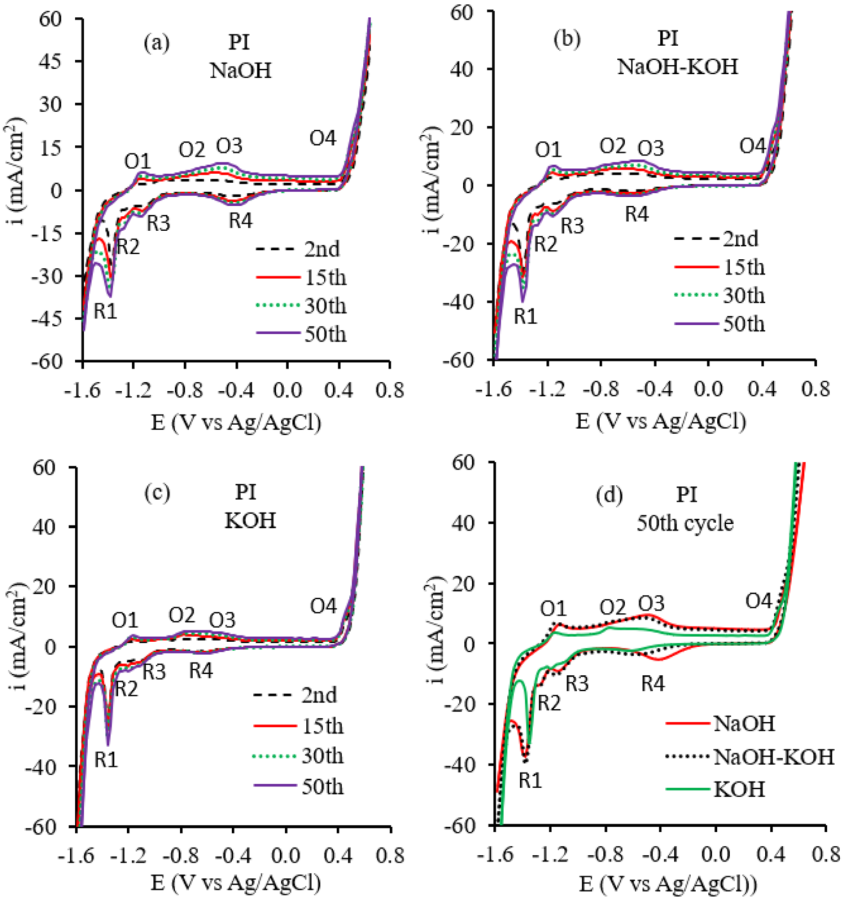

Fig. 1 CV curves of the PI anode in (a) 14 M NaOH, (b) 14 M NaOH/KOH, and (c) 14 M KOH during different cycles. (d) Comparison of the CV curves of the PI anode in the 50th cycle.

overpotential region. This is evidenced by the cathodic charge of the reduction peak O4 (Table 1).

To evaluate and compare ferrate formation, instead of analyzing the anodic charge Q_{O4} associated with ferrate formation at peak O4 (which is difficult to accurately determine due to its location in the oxygen evolution region), the cathodic charge Q_{R4} corresponding to ferrate reduction at peak R4 can be used as an indicator.[20] A greater amount of formed ferrate will lead to an increased subsequent reduction, resulting in a higher charge associated with peak R4. The charge Q_{R4} was determined by integrating peak R4 using the Thales software on the Zahner IM6 electrochemical workstation. The results, summarized in Table 1, show that Q_{R4} is consistently higher when using the PIF electrode compared to the PI electrode. Furthermore, when comparing Q_{R4} across different electrolytes, the highest values were observed in NaOH solution. These findings suggest that the PIF electrode in NaOH provides the most favorable conditions for ferrate synthesis.

Electrochemical impedance spectroscopy (EIS) was conducted to elucidate the electrochemical behavior of PI and PIF electrode surfaces in concentrated alkaline media. Fig. 3a–d present the Bode plots of the PI and PIF electrodes in different electrolytes (14 M NaOH, 14 M NaOH/KOH, and 14 M KOH). From the data given in Fig. 3a and c, the impedance values Z at low-frequency of 10 mHz were determined, with the corresponding results summarized in Fig. 3e. This impedance value encompasses the solution resistance, charge transfer resistance, and diffusion processes. The KOH solution has higher conductivity than the NaOH solution, meaning that the resistance of the KOH solution is lower. However, iron oxides and hydroxides are less soluble in KOH solution,[21] so the 14 M NaOH solution consistently exhibited the lowest Z values for both PI and PIF electrodes. This showed more favorable charge transfer in NaOH, suggesting it as a more suitable medium for electrochemical ferrate synthesis. Furthermore, the PIF electrode exhibited significantly lower Z values (<250 Ω) compared to the PI electrode (700–955 Ω) across all electrolytes. This indicated that PIF possesses enhanced conductivity and facilitates more efficient electrochemical reactions, making it a more favorable material for ferrate electrochemical synthesis.

Fig. 3b shows that only a single peak (60–70°) appears in the mid-frequency range (1–100 Hz) on all phase angle plots for the PI electrode under different electrolyte conditions. This indicates that a single double-layer capacitive behavior occurs on the PI electrode within this mid-frequency range, which is characteristic of electron exchange between the electrode and the electrolyte. In contrast, the PIF electrode exhibits two distinct phase peaks: one in the mid-frequency range (100–150 Hz) and another in the low-frequency range (30–75 mHz). This suggests that, in addition to the double-layer capacitive process

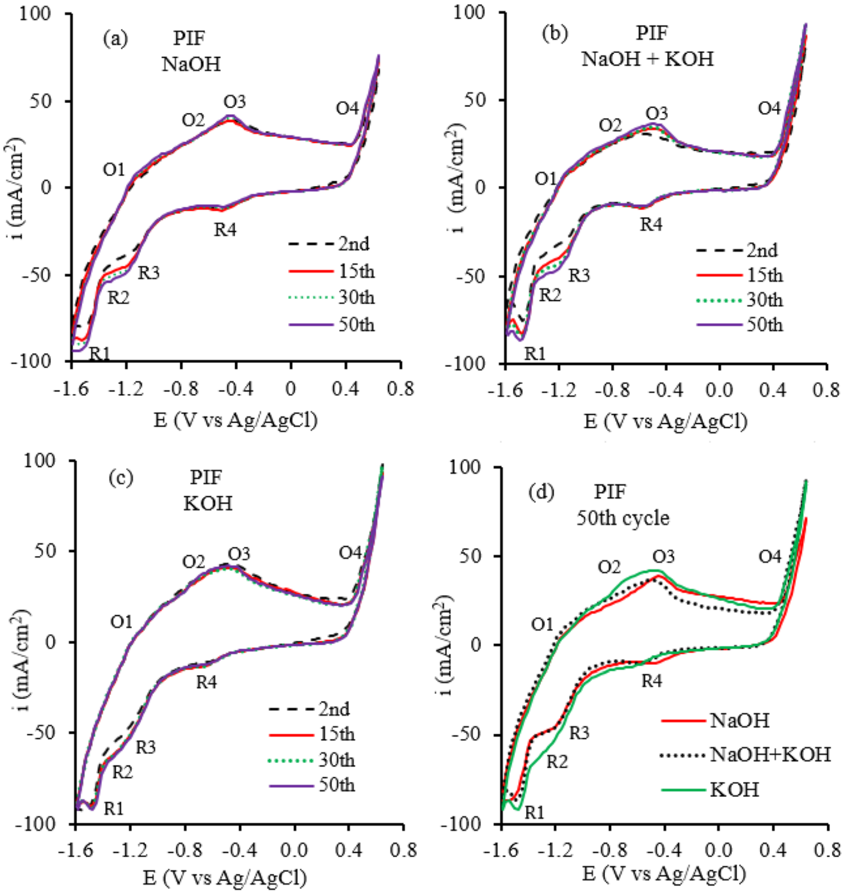

Fig. 2 CV curves of the PIF anode in (a) 14 M NaOH, (b) 14 M NaOH/KOH, and (c) 14 M KOH during different cycles. (d) Comparison of the CV curves of the PIF anode in the 50th cycle.

Table 1 Q_{R4} values (mC) of the PI and PIF anodes in different electrolytes in the 50th cycle

Anode	NaOH	NaOH/KOH	KOH
PI	5.007	3.348	2.133
PIF	5.563	3.615	2.503

observed at the mid-frequency range, a diffusion process into the porous structure of the PIF material occurs at lower frequencies. This result can be explained by the SEM images of the PI and PIF materials prior to electrolysis (Fig. 8a and b). The PI electrode surface appears relatively smooth and homogeneous (Fig. 8a), indicating that only one electrochemical process occurs at the double-layer region. Conversely, the PIF electrode exhibits an uneven surface with small pores (Fig. 8b), suggesting that in addition to the electrochemical process occurring at the outer double-layer region (mid-frequency), ion diffusion into the pores and subsequent reactions at internal active sites take place at lower frequencies.

3.2 Electrochemical synthesis of ferrate

The electrochemical synthesis of ferrate(VI) was conducted under constant current conditions, making current density a critical factor in the efficiency of ferrate formation. Current densities ranging from 16 to 40 mA cm^{-2} were investigated using both PI (pure iron) and PIF (porous iron foam) anodes in different electrolytes, including 14 M NaOH, a NaOH/KOH mixture with a total [OH$^-$] of 14 M, and 14 M KOH. All experiments were carried out at room temperature (20 °C) for 1 hour (Fig. 4).

As Fig. 4 shows, for the PI electrode, the ferrate concentration initially increased with the current density from 16 to 22 mA cm^{-2}, and then declined upon further increase up to 40 mA cm^{-2} in all electrolytes. In particular, NaOH yielded the highest ferrate concentration, approaching 80 mg L^{-1}. The initial increase in the ferrate concentration can be attributed to the greater charge delivery to the electrode surface within a given time, enhancing ferrate production. However, because ferrate formation occurs in the gas evolution region, as suggested by the CV analysis, there is a competitive relationship between ferrate generation and oxygen evolution. Previous studies indicated that increasing current density can lead to greater energy consumption by the water-splitting reaction,[34,35] producing a significant volume of oxygen gas at the anode surface. This gas evolution can hinder contact between the electrode and the electrolyte, thereby limiting the anodic dissolution of iron and reducing the ferrate yield.[35,36] Therefore, the optimal current

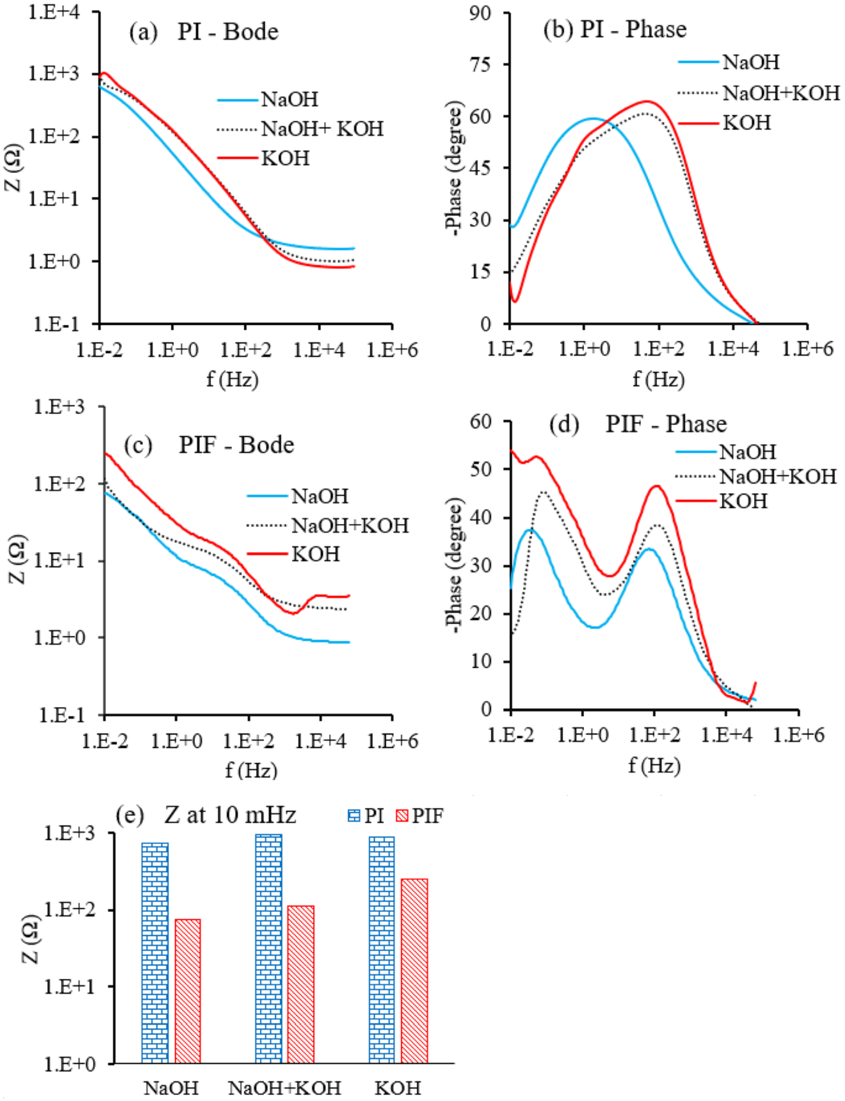

Fig. 3 Bode plots of the (a) impedance magnitude of PI, (b) phase angle of PI, (c) impedance magnitude of PIF, (d) phase angle of PIF. (e) Impedance values of PI and PIF at 10 mHz in different electrolytes.

density for electrochemical ferrate synthesis using the PI electrode was 22 mA cm^{-2} in all examined electrolytes. A similar trend was observed for the PIF electrode; however, the optimal current density for ferrate production was found to be higher at 32 mA cm^{-2}, and the achieved ferrate concentration was 172.8 mg L^{-1}.

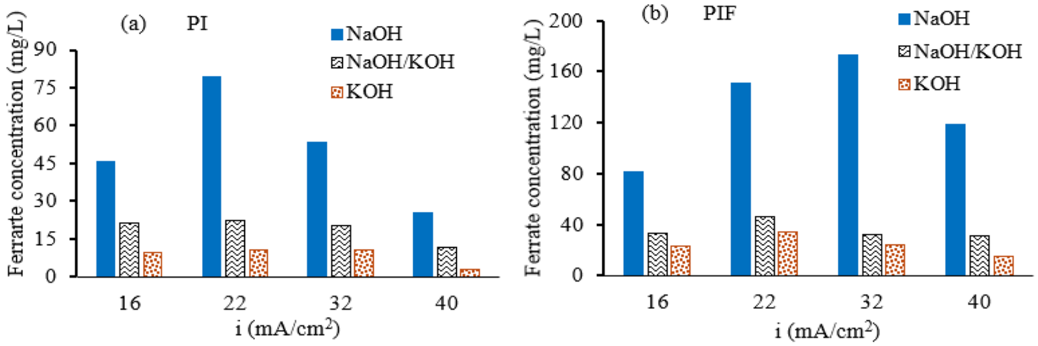

Fig. 4 Effect of current density on the ferrate concentration in different electrolytes using the (a) PI and (b) PIF anodes.

When comparing the performance in different electrolytes, the highest ferrate concentrations for both PI and PIF electrodes were consistently achieved in 14 M NaOH. In contrast, ferrate production in NaOH/KOH and KOH was significantly lower at all tested current densities. The bare potassium ion (K^+) is larger than the bare sodium ion (Na^+), leading to a weaker hydration shell of K^+ ions. Thus, the conductivity of the KOH solution is higher than that of NaOH solutions of the same concentration.[31–33] Both NaOH and KOH solutions can cause passivation on anode surfaces. However, iron oxide/hydroxides are more soluble in NaOH; therefore, higher amounts of ferrate can be obtained in NaOH compared to the KOH electrolyte.[21] The above impedance and CV analyses also demonstrated the less favorable ferrate formation on the anode surfaces in KOH and NaOH/KOH media. Moreover, ferrate is known to decompose more rapidly in KOH compared to NaOH, which further reduces the final ferrate concentration in KOH-based electrolytes.[37] In brief, 14 M NaOH was shown to be the most effective electrolyte for ferrate(VI) synthesis. The optimal current densities were determined to be 22 mA cm^{-2} for the PI electrode and 32 mA cm^{-2} for the PIF electrode. As a result, 14 M NaOH was selected for use in subsequent experiments.

Temperature and electrolysis duration play vital roles in the electrochemical synthesis of ferrate(VI), as they directly affect both the formation of passivation layers on the anode surface and the stability of the synthesized ferrate.[14,38] Elevated temperatures tend to accelerate the reduction of ferrate(VI) to Fe(III), thereby diminishing its yield. Likewise, prolonged electrolysis increases the extent of ferrate decomposition, as some of the freshly formed ferrate may degrade before it can be effectively recovered. These factors collectively contribute to a reduction in the synthesis efficiency. In addition, the duration of electrolysis strongly influences the growth of passivation layers on the anode, which impacts both the electrochemical activity and the long-term performance of the electrode. Fig. 5 demonstrates the effects of temperature (Fig. 5a and b) and electrolysis time (Fig. 5c and d) on the concentration and yield of ferrate(VI) synthesized using PI and PIF anodes in 14 M NaOH.

The PI and PIF anodes exhibit a similar tendency with increasing temperature (Fig. 5a and b). When the temperature increases from 20 °C to 40 °C, both the concentration and yield of ferrate(VI) increase. However, a decline in both parameters is observed when the temperature is further increased to 50 °C. This decrease in performance at 50 °C is primarily attributed to the accelerated thermal decomposition of ferrate(VI) at elevated temperatures. According to Sibel Barisci *et al.*, up to 35.5% of ferrate(VI) decomposed within one hour at 50 °C.[35] The rate of ferrate degradation at this temperature surpassed the rate of its formation, resulting in a decrease in both concentration and yield. Therefore, the optimal temperature for ferrate(VI) synthesis was identified as 40 °C. Notably, the PIF anode consistently outperforms the PI anode in terms of both ferrate(VI) concentration and synthesis efficiency. At 40 °C, the ferrate yield using the PIF anode reached nearly 63%, which was approximately double that achieved with the PI anode. This enhanced performance can be attributed to the improved electron transfer kinetics at the PIF surface, as confirmed by the EIS result. As seen in the SEM image in Fig. 6c, the PIF material's porous structure and numerous surface defects are probably what caused this improvement.

The data of the PIF anode presented in Fig. 5c and d show that, as the electrolysis time increases, the concentration of ferrate(VI) gradually rises. However, the rate of increase slows over time. Moreover, the synthesis efficiency continuously decreases with increasing electrolysis duration. For example, when the electrolysis time is extended from 1 to 20 hours, the ferrate concentration increases from 376 mg L^{-1} to 3580 mg L^{-1}, while the efficiency drops significantly from 63% to 20%. As confirmed by the *E*–*t* curve of the PIF anode in Fig. 7d, no passivation layer forms on its surface. Consequently, the observed decrease in efficiency is due to the decomposition

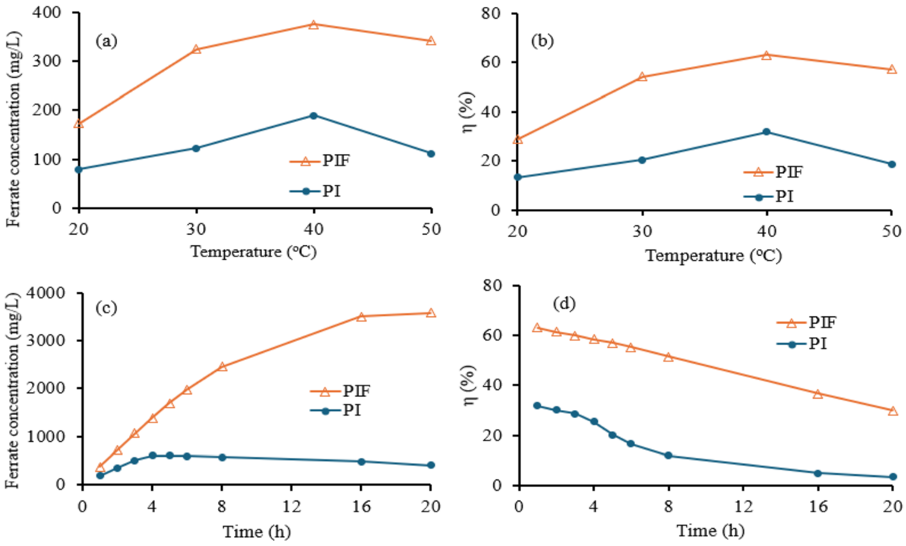

Fig. 5 Effect of (a and b) temperature and (c and d) electrolysis time on ferrate concentration and ferrate generation efficiency.

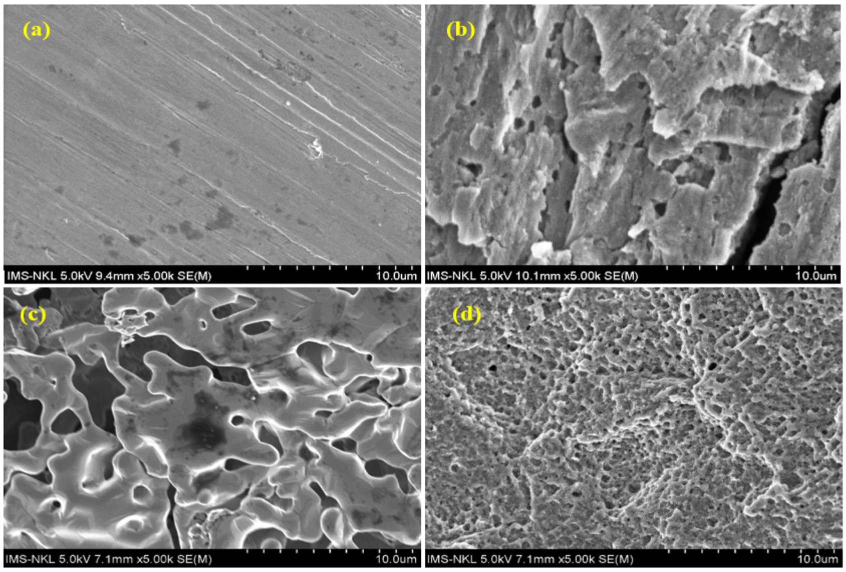

Fig. 6 SEM images of the PI and PIF anodes before (a and b) and after 20 h electrolysis (c and d).

of ferrate(VI) during prolonged electrolysis. In contrast, for the PI anode, the ferrate concentration increases rapidly within the first 1 to 3 hours, while the efficiency simultaneously declines. However, as the electrolysis time is further extended to 5 hours, the increase in the ferrate concentration becomes marginal, accompanied by a more pronounced decrease in the synthesis

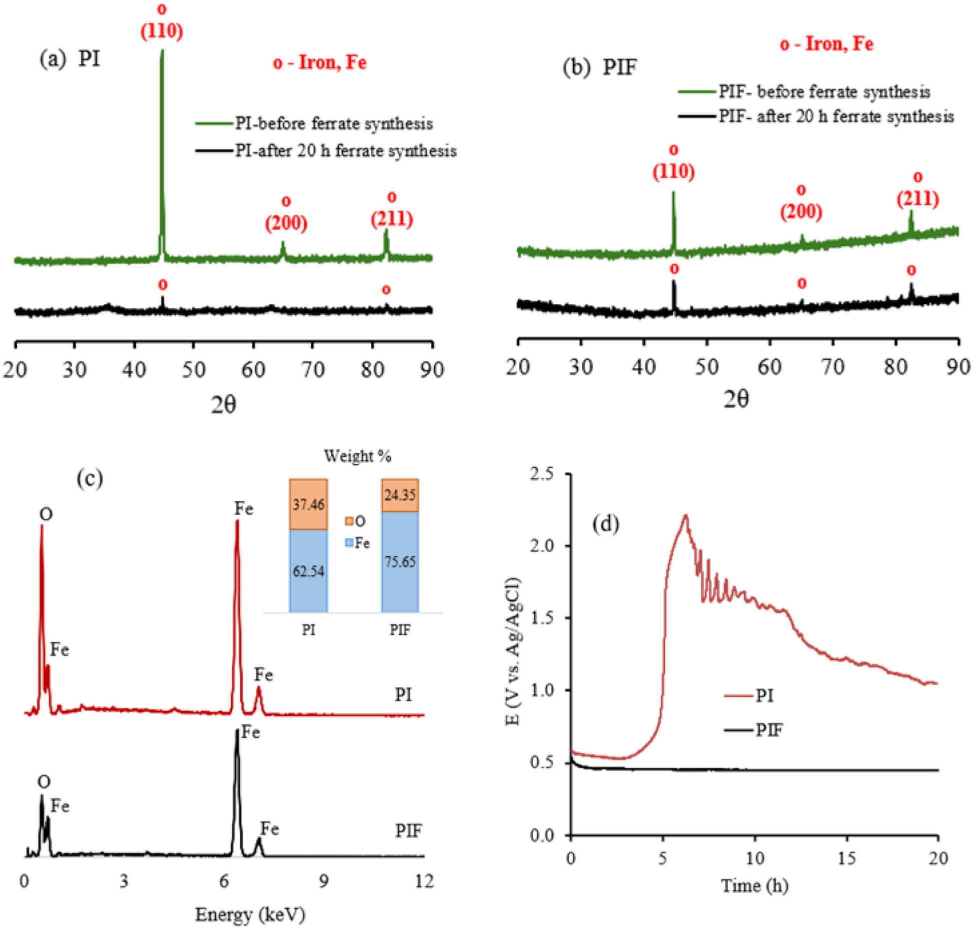

Fig. 7 XRD patterns before and after 20 h electrolysis of (a) PI and (b) PIF. (c) EDS of PI and PIF after 20 h electrolysis. (d) *E*–*t* curves of PI and PIF during 20 h electrolysis.

efficiency. Especially, after 5 hours of electrolysis, not only does the efficiency significantly drop, but the ferrate concentration also begins to decrease. This phenomenon is attributed to the progressive formation of a passivation layer on the PI anode over time. The formation of this passive film is supported by the gradual increase in the response potential observed in the *E*–*t* curve of PI after 3 hours of electrolysis, followed by a sharp rise after 5 hours (Fig. 7d). This thick passivation layer hinders electrochemical reactions at the anode surface, thereby significantly suppressing ferrate formation on the PI electrode. Thus, the ferrate synthesis process using the PIF anode was superior to that using the PI anode.

3.3 Characteristics of the anode surface before and after ferrate synthesis

The morphological and structural characteristics of the anode materials affect the electrochemical behavior and ferrate electrochemical synthesis efficiency. The SEM images, XRD, and EDS of the PI and PIF anodes were investigated. The surface of the PI anode given in Fig. 6a appears smooth and uniform. There are no significant signs of porosity, cracks, or surface roughness at this magnification (×5000). The absence of prominent surface defects suggests a compact microstructure, which may correlate with limited surface reactivity or restricted electrolyte diffusion in electrochemical applications. Fig. 6c shows the PIF anode surface, which has a highly porous structure with interconnected pores of various sizes, allowing the electrolyte to penetrate deeply into the electrode matrix. This significantly enhances the interfacial contact area between the anode and the electrolyte, thereby facilitating the ferrate formation process. The irregular pore edges and sharp features suggest regions of structural imperfection that may serve as active sites for electrochemical reactions under applied current. The SEM image analysis demonstrated the superiority of the PIF anode over PI in the electrochemical synthesis of ferrate, which is consistent with the above research results. A similar result was proven in a previous study,[17] where the sponge iron with a loosely packed structure and high porosity was more beneficial for the ferrate synthesis than grey cast iron with a dense, compact morphology.

After electrolysis, the anode surface undergoes morphological changes due to electrochemical corrosion, ferrate formation, and the accumulation of intermediate species that may lead to the development of a passive layer. SEM images after 20 hours of electrolysis (Fig. 6b and d) show that the PIF electrode develops increased porosity as a result of iron dissolution, while the PI electrode surface becomes increasingly covered by a passive film, which may inhibit further electrochemical reactions. To study the formation of a passivation layer on the surface of PI and PIF electrodes during the synthesis of ferrate, some measurements (including XRD, EDS and *E*–*t* curves) were performed.

Fig. 7a and b present the XRD patterns of the PI and PIF electrodes before and after 20 hours of ferrate synthesis. The XRD patterns of both materials prior to electrolysis show three characteristic peaks at 2θ angles of 44.82°, 65.16°, and 82.60°, corresponding to the (110), (200), and (211) diffraction planes of metallic iron, respectively, according to JCPDS card no. 00-006-0696. However, the peak intensities for PI are significantly higher than those of PIF, likely due to the presence of numerous pores on the PIF surface, which disrupt the crystallinity and reduce the material's ability to diffract X-rays effectively. After 20 hours of electrolysis, the characteristic peaks of metallic iron in the PI electrode decrease markedly in intensity. For the PIF material, the intensity of the iron diffraction peaks shows a slight decrease after 20 hours of electrolysis, which is attributed to the formation of intermediate products on the electrode surface during ferrate synthesis. The EDS spectrum of PIF after 20 hours of electrolysis (Fig. 7c) revealed the presence of oxygen and iron on the PIF surface, with oxygen accounting for nearly 25 wt%, demonstrating the existence of iron oxide species. Comparing the surface compositions of PI and PIF after 20 hours of synthesis, iron remained the dominant element on PIF (75.65 wt%), whereas on PI, the iron content dropped to

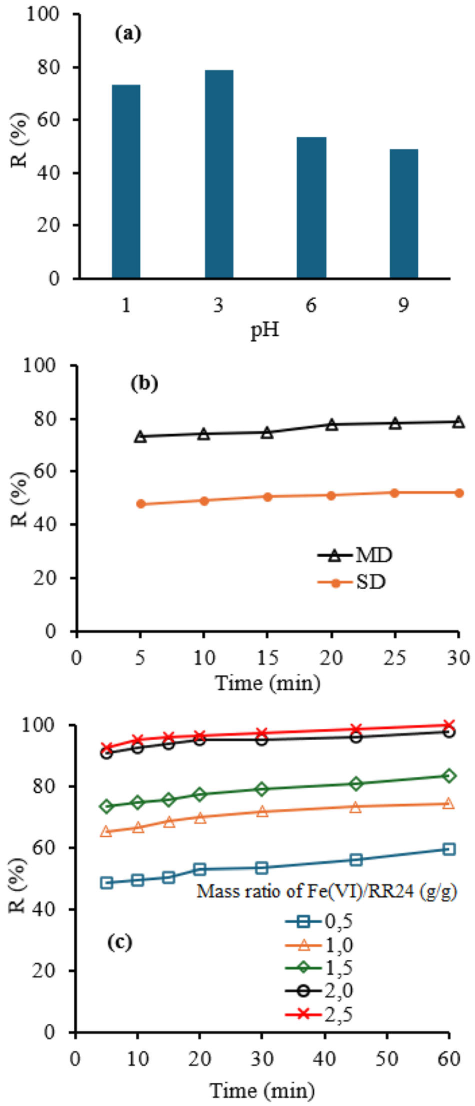

Fig. 8 Effect of (a) pH, (b) treatment method, and (c) ferrate/RR24 mass ratio on the RR24 removal efficiency.

Table 2 Comparison of dye treatments using ferrate

Dyes	Conditions	Treatment time (minutes)	Removal efficiency (%)	References
Reactive brilliant red X-3B	[Fe(VI)] = 75 mg L^{-1}, [dye] = 50–200 mg L^{-1}, pH 4–9	30	77.6–98.0	12
Methylene blue	[Fe(VI)] = 59.9 mg L^{-1}, [dye] = 50 mg L^{-1}, pH 13.6	35	96.8	44
Remazol black B	Molar ratio of Fe(VI)/dye = 5/1, pH 8	120	>95.0	45
Metanil yellow	Molar ratio of Fe(VI)/dye = 2/1, pH 8	25	92.4	46
Congo red	Molar ratio of Fe(VI)/dye = 5/1, pH 9.2	20	98.2	47
Reactive red 195	Molar ratio of Fe(VI)/dye = 30/1, pH 3	3	96.3	13
Methylene blue	Molar ratio of Fe(VI)/dye = 10/1, pH 3	5	93.0	19
Textile wastewater	[Fe(VI)] = 40 mg L^{-1}, COD 6980 mg L^{-1}, pH 9	30	83.0% COD	48
Textile wastewater	[Fe(VI)] = 150 mg L^{-1}, COD 550–1000 mg L^{-1}, pH 6.5–8.5	20	90.0% COD	43
Reactive red 24	Mass ratio of Fe(VI)/dye = 2/1, pH 3	5	>90.0	This study
		30	98.0	

62.54 wt%. These data indicated that the accumulation of intermediate products on the PI surface was more significant than that on the PIF surface. This accumulation led to the formation of a poorly conductive passivation layer on the PI anode, which blocked active sites and impeded electrochemical reactions. The sharp increase in the response potential on the polarization curve of PI in Fig. 7d after just 4 hours of electrolysis was evident of a passivation layer on the PI anode.[17,18] In contrast, the response potential of the PIF electrode remained stable throughout the electrolysis process, indicating that the passive layer formed on this anode surface was negligible and did not affect the electrochemical synthesis of ferrate. A similar study on the ferrate electrochemical synthesis using a sponge iron anode showed a stable *E*–*t* polarization curve throughout the 30 hour electrolysis period under the synthesis conditions of 50 °C and a current density of 30 mA cm^{-2}.[17] As a result, the PIF electrode maintained efficient and sustained ferrate synthesis, whereas the PI electrode experienced decreased activity and increased energy consumption due to passivation.

The results of SEM, XRD, and EDS prove that PIF is a suitable anode material for the electrochemical synthesis of ferrate. For continuous electrochemical ferrate(VI) generation, the PIF anode's lack of a passive layer is very beneficial since it avoids interruptions from electrode surface treatment and lowers the operating expenses related to electrode maintenance. The ferrate prepared in 14 M NaOH using the PIF anode was then used to treat azo dye, reactive red 24, in the following section.

3.4 Removal of azo dye RR24 by generated ferrate

pH plays a crucial role in the dye treatment process using ferrate, as it directly influences ferrate's oxidative capacity.[39,40] Fig. 8a illustrates the effect of pH on the removal efficiency of RR24. The results show that ferrate exhibits a higher removal efficiency for RR24 under acidic conditions compared to alkaline conditions. In an acidic medium, the removal efficiency exceeds 70%, whereas under alkaline conditions, it only reaches around 50%. This is attributed to the significantly stronger oxidative potential of ferrate in acidic medium, where the redox potential reaches 2.2 V, in contrast to only 0.72 V in alkaline medium.[41,42]

The MD procedure demonstrated the significantly higher efficiency in the treatment of RR24 compared to the SD procedure (Fig. 8b). After 30 minutes of treatment, the MD approach achieved nearly 80% removal efficiency, while the SD method reached only 53%. This indicated that dividing the ferrate into smaller portions enhanced the oxidation of the dye, likely by minimizing the self-decomposition of ferrate during the reaction process. The MD method was applied to study the effect of the ferrate/RR24 mass ratio on RR24 treatment. Fig. 8c suggests that the dye degradation reaction occurs very rapidly, with the majority of decomposition taking place within the first few minutes. At the ferrate-to-dye mass ratio of 1 g g^{-1}, the removal efficiency reached 65% within the first five minutes, but only increased to approximately 74% after 60 minutes. Comparing the removal efficiencies of RR24 at different ferrate/RR24 mass ratios, it was observed that increasing the ferrate dose from 0.5 to 2 g g^{-1} led to a significant improvement in the removal efficiency. However, further increasing the ratio to 2.5 g g^{-1} resulted in only a marginal change over time. At the mass ratio of 2 g g^{-1}, more than 90% of the dye was removed within 5 minutes, and nearly 98% was achieved after 30 minutes. These results suggest that the ferrate/RR24 mass ratio of 2 g g^{-1} is the optimal dosage required for the nearly complete removal of RR24.

The data presented in Table 2 demonstrate that ferrate is capable of effectively treating a wide range of dyes from various classes, including reactive dyes (reactive red 195, reactive brilliant red X-3B, *etc.*), direct dyes (Congo Red), and acid dyes (Metanil Yellow). These studies reported that dye removal using ferrate was a simple and highly efficient process, with rapid treatment times typically ranging from 20 to 30 minutes. Some studies have shown that ferrate can remove more than 90% of dye content within as little as 3–5 minutes.[13,19] In published work,[43] the application of ferrate in textile wastewater treatment achieved up to 90% removal of chemical oxygen demand (COD). These findings highlight the significant potential of ferrate for practical applications in textile wastewater treatment.

4. Conclusions

This study demonstrated that the PIF with a highly porous structure was a suitable anode material for the electrochemical synthesis of ferrate. The optimal conditions for ferrate generation using PIF were identified as 14 M NaOH at 40 °C with a current density of 32 mA cm^{-2}. Under this condition, the ferrate(VI) production efficiency reached up to 63%. The CV and EIS analysis also indicated that the electrochemical properties of the PIF anode in 14 M NaOH were favorable for ferrate synthesis. The results of SEM, XRD, EDS, and *E*–*t* curves showed that the passive layer formed on the PIF anode surface was insignificant and had no impact on the electrochemical synthesis of ferrate. The synthesized ferrate using the PIF anode almost completely removed RR24, with a removal efficiency of over 98% at pH 3 and a ferrate/RR24 mass ratio of 2 g g^{-1}.

Author contributions

Thi Van Anh Nguyen: Writing—original draft, formal analysis, methodology; Thị Xuan Mai: data analysis, The Duyen Nguyen: methodology; Minh Quy Bui: methodology, Hoang Yen Phan: data analysis, Thi Thanh Thuy Mai: writing—review and editing, methodology, formal analysis, and project administration.

Conflicts of interest

There are no conflicts to declare.

Data availability

The authors confirm that the data supporting the findings of this study are available within the article.

Acknowledgements

This research was financially supported by the Vietnam Academy of Science and Technology under code number UDPTCN.10/25-27 and the Vingroup Innovation Foundation under code number VINIF.2024.TS.027.

References

1 S. Khan, A. Malik, *Environmental Deterioration and Human Health: Natural and Anthropogenic Determinants*, 2014, 55–71.
2 W. U. Khan, S. Ahmed, Y. Dhoble and S. Madhav, *J. Indian Chem. Soc.*, 2023, **100**(1), 100829.
3 D. Yaseen and M. Scholz, *Int. J. Environ. Sci. Technol.*, 2019, **16**, 1193–1226.
4 S. Z. Hashmi, J. Dwivedi, D. Kishore and A. E. Kuznetsov, *J. Mol. Struct.*, 2023, **1278**, 134922.
5 D. Bareth, S. Jain, J. Kumawat, D. Kishore, J. Dwivedi and S. Z. Hashmi, *Bioorg. Chem.*, 2024, **143**, 106971.
6 T. Sarwar and S. Khan, Textile industry: pollution health risks and toxicity, in *Textile Wastewater Treatment: Sustainable Bio-Nano Materials and Macromolecules*, Springer, 2022, vol. 1, pp. 1–28.
7 N. Hemashenpagam and S. Selvajeyanthi, Textile dyes and their effect on human beings, in *Nanohybrid Materials for Treatment of Textiles Dyes*, Springer, 2023, pp. 41–60.
8 S. Barışçı, O. Turkay and A. Dimoglo, *Ferrites and Ferrates: Chemistry and Applications in Sustainable Energy and Environmental Remediation*, ACS publication, 2016, pp. 349–409.
9 V. K. Sharma, R. Zboril and R. S. Varma, *Acc. Chem. Res.*, 2015, **48**(2), 182–191.
10 J. Q. Jiang, *J. Chem. Technol. Biotechnol.*, 2014, **89**(2), 165–177.
11 A. Yaghoot-Nezhad, E. Saebnoori, I. Danaee, S. Elahi, N. B. Panah and M. R. Khosravi-Nikou, *J. Water Process Eng.*, 2022, **49**, 103017.
12 Q. Han, W. Dong, H. Wang, T. Liu, F. Sun, Y. Ying and X. Yan, *Sep. Purif. Technol.*, 2013, **108**, 74–82.
13 T. V. A. Nguyen, T. T. T. Mai, T. B. Phan, H. Q. Tran and M. Q. Bui, *J. Chem. Technol. Biotechnol.*, 2024, **99**(11), 2454–2463.
14 Z. Mácová, K. Bouzek, J. Híveš, V. K. Sharma, R. J. Terryn and J. C. Baum, *Electrochim. Acta*, 2009, **54**(10), 2673–2683.
15 D. Tiwari, Ferrate (VI) a greener solution: Synthesis, characterization, and multifunctional use in treating metal-complexed species in aqueous solution, in *Ferrites and Ferrates: Chemistry and Applications in Sustainable Energy and Environmental Remediation*, ACS Publications, 2016, pp. 161–220.
16 M. Alsheyab, J.-Q. Jiang and C. Stanford, *J. Hazard. Mater.*, 2009, **90**(3), 1350–1356.
17 X. Sun, K. Zu, H. Liang, L. Sun, L. Zhang, C. Wang and V. K. Sharma, *J. Hazard. Mater.*, 2018, **344**, 1155–1164.
18 T. T. T. Mai, T. V. A. Nguyen, T. B. Phan and T. G. Le, *J. Electrochem. Soc.*, 2023, **170**(8), 083510.
19 T. T. T. Mai, T. V. Anh Nguyen and T. B. Phan, *J. Appl. Electrochem.*, 2024, **54**(8), 1783–1794.
20 L. Nikolić-Bujanović, M. Čekerevac, M. Vojinović-Miloradov, A. Jokić and M. Simičić, *J. Ind. Eng. Chem.*, 2012, **18**(6), 1931–1936.
21 M. Diaz, K. Doederer, J. Keller, M. Cataldo, B.-C. Donose, Y. Ali and P. Ledezma, *J. Electroanal. Chem.*, 2021, **880**, 114897.
22 M. Čekerevac, M. Simičić, L. N. Bujanović and N. Popović, *Corros. Sci.*, 2012, **64**, 204–212.
23 Z. Ding, C. Yang and Q. Wu, *Electrochim. Acta*, 2004, **49**(19), 3155–3159.
24 M. Karami, H. Koohestani and H. Gholami, *Int. J. ISSI*, 2022, **19**(1), 15–19.
25 Z. Xu, X. Ma, F. He, M. Lu, J. Zhang, S. Wang, P. Dong and C. Zhao, *J. Hazard. Mater.*, 2024, **465**, 133193.
26 Z. Mácová and K. Bouzek, *J. Appl. Electrochem.*, 2012, **42**, 615–626.
27 F. Lapicque and G. Valentin, *Electrochem. Commun.*, 2002, **4**(10), 764–766.
28 W. Yang, Y. Zhou, H. Wang and D. Bi, *Russ. J. Electrochem.*, 2009, **45**, 795–799.
29 N. T. Van Anh, P. T. Binh, M. T. Xuan and M. T. T. Thuy, *Vietnam J. Chem.*, 2024, **62**(4), 437–445.
30 L. Hrnčiariková, M. Gál, K. Kerekeš and J. Híveš, *Electrochim. Acta*, 2013, **110**, 581–586.

31 R. Mancinelli, A. Botti, F. Bruni and M. A. Ricci, *J. Phys. Chem. B*, 2007, **111**, 13570–13577.

32 S. H. Ma, Z. Y. Jiao, T. X. Wang and Z. X. Yang, *Eur. Phys. J. B*, 2010, **75**, 469–474.

33 R. Mancinelli, A. Botti, F. Bruni, M. A. Ricci and A. K. Soper, *J. Phys. Chem. B*, 2007, **111**(48), 13570–13577.

34 S. Samimi-Sedeh, E. Saebnoori and A. Hassanzadeh, *Adv. Mater. Processes*, 2019, **7**(4), 3–15.

35 S. Barışçı, F. Ulu, H. Särkkä, A. Dimoglo and M. Sillanpää, *Int. J. Electrochem. Sci.*, 2014, **9**(6), 3099–3117.

36 X. Yu and S. Licht, *J. Appl. Electrochem.*, 2008, **38**, 731–742.

37 J.-J. Xu, J.-M. Wang, W.-H. Yang, C. Chen and J.-Q. Zhang, *J. Electrochem.*, 2004, **10**(1), 15.

38 J. Quino-Favero, A. G. Espinoza, E. Saettone, J. C. Y. Llanos and F. P. Larroca, *Heliyon*, 2024, **10**(15), e35414.

39 D. Wang, Z. Zeng, H. Zhang, J. Zhang and R. Bai, *Chem. Eng. J.*, 2022, **431**, 133381.

40 T. Kamachi, T. Kouno and K. Yoshizawa, *J. Org. Chem.*, 2005, **70**(11), 4380–4388.

41 V. K. Sharma, *Adv. Environ. Res.*, 2002, **6**(2), 143–156.

42 R. Sarma, A. M. Angeles-Boza, D. W. Brinkley and J. P. Roth, *J. Am. Chem. Soc.*, 2012, **134**(37), 15371–15386.

43 I. Ciabatti, F. Tognotti and L. Lombardi, *Desalination*, 2010, **250**(1), 222–228.

44 O. Turkay, S. Barışçı and A. Dimoglo, *Sep. Sci. Technol.*, 2016, **51**(11), 1924–1931.

45 N. B. A. Prasetya, S. Suripto, A. Haris, N. Ngadiwiyana and N. S. Mohammed, *J. Phys.: Conf. Ser.*, 2021, **1943**, 012181.

46 G. Gunawan, N. B. A. Prasetya, A. Haris and F. Febriliani, *J. Phys.: Conf. Ser.*, 2021, **1943**, 012181.

47 S. Fatimah, S. Widyawati, N. Jannah and A. Mei, *J. Phys.: Conf. Ser.*, 2021, **1858**, 012060.

48 S. N. Malik, P. C. Ghosh, A. N. Vaidya, V. Waindeskar, S. Das and S. N. Mudliar, *Water Sci. Technol.*, 2017, **76**(5), 1001–1010.